Available online at www.sciencedirect.com

ScienceDirect

IFAC Papers Online CONFERENCE PAPER ARCHIVE

IFAC-PapersOnLine 48-28 (2015) 1477–1482

Benchmark Data on a Linear Time- and Parameter-varying system ⋆

J. Lataire, E. Louarroudi, R. Pintelon and Y. Rolain *

* *Vrije Universiteit Brussel (VUB), Dept. ELEC, Pleinlaan 2, 1050 Brussels, Belgium (e-mail:* jlataire@vub.ac.be*)*

Abstract: This article describes benchmark data for time- and parameter varying systems, from measurements conducted at the ELEC department, Vrije Universiteit Brussel. The system is an electronic bandpass filter, the resonance frequency of which can be varied in a controlled fashion. The signal that controls the resonance frequency is provided (and can be interpreted as a scheduling variable), along with the measured input and output signals, and the signals stored into the arbitrary waveform generator. The system is suitably modelled as a Linear Parameter Varying system, or as a Linear Time-Varying system if the scheduling variable is not used. The measurements are conducted in a low-noise environment, allowing for a Signal-to-Noise-Ratio of more than 60 dB. The system is mainly linear in its input-output relation, although some nonlinear effects are visible. The data includes different typical excitation scenarios, including band-limited noise, random phase multisines with sparse excited frequencies, piecewise constant scheduling, and slow, medium and fast varying scheduling. The data sets are available at the IFAC TC1.1 repository: http://tc.ifac-control.org/1/1/Data%20Repository.

Keywords: Benchmark data, Linear system, Time-Varying system, Parameter Varying system, Electronic bandpass filter

1. MOTIVATION

A lot of practical examples in engineering applications have an approximately linear input-output behaviour, which depends on some external factor or parameter. Think for instance of positioning systems, the dynamics of which depend on the instantaneous setpoint (Tóth et al., 2011), an impedance measurement of a metal subject to an electrochemical process (Breugelmans et al., 2012), or the structural modes of an airborne airplane which depend on the flight height and speed (Fujimori and Ljung, 2006; Ertveldt et al., 2014).

For this type of systems, LTI (Linear Time Invariant) models are too restrictive. However, a full-blown nonlinear model is likely to be unnecessarily laborious to identify and analyse. Linear time-varying (LTV) and Linear Parameter Varying (LPV) models form a attractive compromise. Namely, they are sufficiently rich to capture the variability of the dynamics, while constructing robust control strategies remains tractable (Balas, 2002; Caigny et al., 2010). Plenty of identification tools are found in the literature, for LTV systems (Spiridonakos and Fassois, 2009; Niedzwiecki, 2008; Verhaegen and Yu, 1995), and for LPV systems (Hsu et al., 2008; Tóth et al., 2009; Bamieh and Giarre, 2002).

This article describes a benchmark data set obtained from measurements on a fairly simple parameter varying electronic circuit. On this dataset, the user can test whether his/her identification tool is usable on a real-world system, which satisfies in very good approximation the basic assumptions for LPV systems: input-output linearity. In addition, a *static dependence on the scheduling* already gives very good results on the presented measurement data, such that relatively simple LPV model structures can be used, as will be demonstrated in the results section. Although for all measurements the scheduling signal is provided, the user can choose not to use it during the identification, and identify an LTV model instead.

The remainder of this article is structured as follows. Sections 2 and 3 respectively describe the system to be identified, and the setup used to make the measurements. Section 4 describes the available data sets, including the different excitation and scheduling signals applied during the experiments, and benchmark criteria for LTV and LPV estimators. Section 5 provides some identification results on the data sets.

2. CONSIDERED SYSTEM

The considered system is an electronic filter, the schematic of which is given in Figure 1. It is a second order bandpass filter with one variable resistance, implemented as a parallel connection of an n-type J-FET transistor (type BF245B) and a 470 kΩ resistor. The scheduling variable $p(t)$ is the gate-source voltage of the transistor. It should be negative because the transistor has an n-type depletion channel. Its resistance increases when $p(t)$ increases in amplitude.

A qualitative description of the dynamic behaviour of the circuit follows from basic derivations in electrical network theory. We have that, for a constant scheduling signal $p(t) = p^*$, the voltage transfer function $Y(s)/U(s)$ (i.e. the ratio of

⋆ This work is sponsored by the Research Foundation Flanders (FWO-Vlaanderen), the Flemisch Government (Methusalem Fund, METH1), the Belgian Federal Government (Interuniversity Attraction Poles programme, DYSCO)

2405-8963 © 2015, IFAC (International Federation of Automatic Control) Hosting by Elsevier Ltd. All rights reserved.
Peer review under responsibility of International Federation of Automatic Control.
10.1016/j.ifacol.2015.12.342

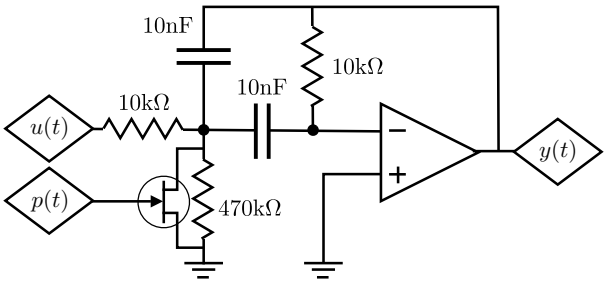

Fig. 1. Electric schematic of the LPV circuit. The OPAMP was of the type TL071CN, and the transistor BF245B.

Laplace transforms of the output and input signals, with s the Laplace variable) has a zero at the origin, and one pair of complex conjugate poles. Only the imaginary parts of the latter depend on p^*. Lower values of $|p^*|$ yield higher values of the imaginary parts (in absolute value) of the poles and, thus, increased resonance frequencies.

This dynamic behaviour is verified with measurements with constant scheduling signals. The results are given in Figure 2. The transfer function and associated poles and zeroes are plotted, where each shade of gray corresponds to a constant value of the scheduling signal p, expressed in Volts (V). Indeed, the poles are moving along lines parallel to the imaginary axis, towards higher frequencies for lower amplitudes of p. The measurements used for this plot are available, see further on.

It is clear that the identification problem becomes more challenging if the scheduling signal $p(t)$ is non-constant during an experiment. In that case, an LTI model will be insufficient to capture the resulting time-varying dynamic behaviour. Two approaches are considered: either the scheduling signal is considered to be unknown and the system is modelled as time-varying, or the scheduling signal is included in the modelling process and the system is modelled as parameter varying.

Also, and just like for any practical real-world system, the input-output behaviour of this circuit is only approximately linear. It will be shown, based on measurements, that contributions from nonlinear effects are detectable in the circuit's response.

3. MEASUREMENT SETUP

The electronic filter described in the previous section is measured with the VXI measurement setup depicted in Figure 3. The input and scheduling signals u_{ref} and p_{ref} are generated with arbitrary waveform generators of type HP E1445A (output impedance of 50 Ω, and internal reconstruction filter with cut-off frequency at 250 kHz enabled), and applied directly to the input and scheduling ports of the circuit. The applied input and scheduling signals, and resulting output signal are buffered (input impedance larger than 5 MΩ, output impedance of 50 Ω) and measured with the acquisition cards of type HP E1430A, which are properly anti-alias protected. The generator and acquisition cards are synchronised and operate at the same sampling frequency of $f_s = 10\,\text{MHz}/2^6 \approx 156\,\text{kHz}$. This measurement setup yields a very high signal-to-noise ratio, typically up to 80 dB, as will be shown.

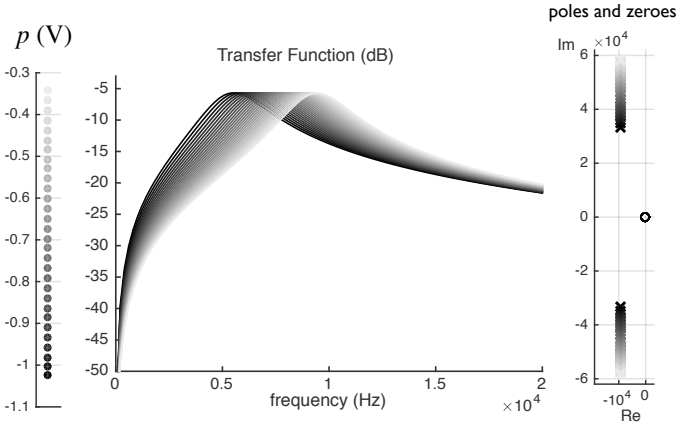

Fig. 2. Middle plot: estimated transfer functions of the system, for different values of the constant scheduling variable (left figure). Right plot: corresponding poles x and zero o.

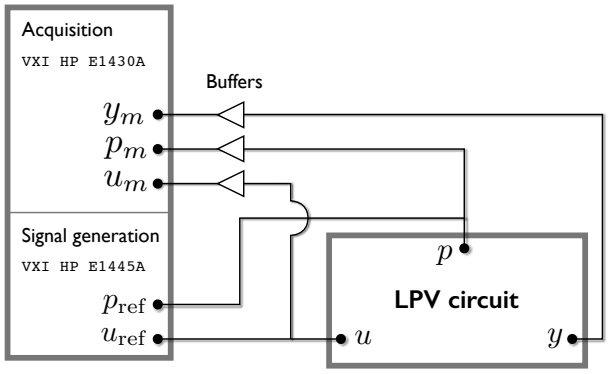

Fig. 3. Measurement setup. Generator cards have an output impedance of 50 Ω. The buffers have an input impedance larger than 5 MΩ.

4. BENCHMARK DATA SETS

4.1 Excitation signal

The reference excitation signal u_{ref} is constructed as a sum of cosines

$$u_{\text{ref}}(t) = \sum_{k=1}^{N_{\max}} A_k \cos(\omega_k t + \varphi_k), \qquad \omega_k = \frac{2\pi k f_s}{N} \tag{1}$$

where N is the number of samples in a period, the phases φ_k are uniformly distributed in $[0, 2\pi[$, and $N_{\max}$ is chosen such that the upper bound of the excited frequency band is $\omega_{N_{\max}} \approx 2\pi\,20\text{kHz}$. For the amplitudes A_k, a distinction is made as follows:

Multisine: A significant amount of amplitudes A_k are set to zero. The others are all equal. Thus, a set of *excited bins*[1] is defined as $\mathbb{K}_{\text{exc}} \subset \{1, \ldots, N_{\max}\}$, where $A_k \neq 0, \forall k \in \mathbb{K}_{\text{exc}}$.

Periodic noise: A_k is zero-mean, independently and identically, Rayleigh distributed over k.

In addition, A_k is scaled such as to obtain a desired RMS value of the excitation signal. As a result, the amplitudes of

[1] The bin is a normalised frequency unit: 1 bin corresponds to $\omega_1 = 2\pi f_s/N$.

the multisine, given their sparseness, will typically be larger than those of the periodic noise.

During the measurements, the applied excitation signal will be repeated periodically, allowing the system to reach a steady-state. As such, and for a synchronised periodic scheduling signal (see next section), the response of the system will be periodic as well. This conveniently allows for a determination of the noise level. Three full periods are measured, that is, $3N$ data points are acquired per experiment.

For the multisine excitation, a further refinement is performed. Namely, the excited bins are all multiples of $P_{\text{exc}} \in \mathbb{N}_\circ$, such that one period of the multisine fits exactly P_{exc} times in N data points. This leaves plenty of non-excited frequencies between each pair of excited ones, and allows us to obtain a non-parametric estimate of the instantaneous transfer function, see Lataire et al. (2012) and demonstrated further on. In addition, only *odd* multiples of P_{exc} are excited, and some of them are randomly removed. This procedure provides information on the (small) nonlinear distortions, generated by the circuit (Pintelon et al., 2013; Schoukens et al., 2009). In summary for the multisine excitation, the set of excited frequency bins is given by

$$\mathbb{K}_{\text{exc}} = \left(\{P_{\text{exc}}, 3P_{\text{exc}}, 5P_{\text{exc}}, \dots\} \cap \{1, \dots, N_{\max}\}\right) \setminus \mathbb{K}_{\text{remove}}$$

where $\mathbb{K}_{\text{remove}}$ is a set of randomly (uniform) chosen bins.

4.2 Scheduling signal

For the scheduling signal, the following modes are used

Constant: 30 equidistant constant values are applied as scheduling input, during successive experiments. Thus, during each experiment the circuit can be assumed to behave time invariantly. These measurements, with a multisine excitation, were used to obtain the plots in Figure 2.

Ramp: A linearly increasing signal is applied, covering the range of voltage values $[-1.05, -0.35]$ V in N data points. This yields a gradual variation of the dynamics.

Harmonic: A sum of sines with random amplitudes and phases is applied, where a limited amount of bins are excited, namely 1, 3, or 20. Formally,

$$p_{\text{ref}}(t) = V_{\text{DC}} + \sum_{k=1}^{h} B_k \cos(\omega_k t + \phi_k), \quad \omega_k = \frac{2\pi k f_s}{N} \tag{2}$$

with $h \in \{1, 3, 20\}$ and where the amplitudes B_k are zero-mean, randomly normally distributed. Note that $p_{\text{ref}}(t)$ has the same periodicity as $u_{\text{ref}}(t)$ in (1). The (negative) offset $V_{\text{DC}} = -700$ mV is added to keep the scheduling signal within a relevant range. The scheduling signal is scaled to a fixed peak-to-peak value, see further on.

An example time domain plot of each such a scheduling signal is given in Figure 4.

4.3 Available data sets

An overview of the available data sets is given in Table 1. Note that each row corresponds to 4 data sets (at most), with the following possible combinations of the RMS of the excitation signal, and peak-to-peak (P2P) value of the scheduling signal:

u	p	P_{exc}	N	R_u	R_p	n_{exc}	h	f_h (Hz)
MS	Const.	10	15640	1	30	75	n.a.	0
MS	Ramp	10	15640	3	1	75	n.a.	–
MS	Harm.	10	15640	3	2	75	1	9.99
MS	Harm.	10	15640	3	2	75	3	29.97
MS	Harm.	10	15640	3	2	75	20	199.81
MS	Harm.	4	1568	3	2	21	3	298.95
MS	Harm.	4	1568	3	2	21	20	1992.98
PN	Const.	-	15640	1	30	1993	n.a.	0
PN	Ramp	-	15640	3	1	1993	n.a.	-
PN	Harm.	-	15640	3	2	1993	1	9.99
PN	Harm.	-	15640	3	2	1993	3	29.97
PN	Harm.	-	15640	3	2	1993	20	199.81
PN	Harm.	-	1568	3	2	201	3	298.95
PN	Harm.	-	1568	3	2	201	20	1992.98

Table 1. Available data sets. MS: multisine, PN: periodic noise. P2P: peak-to-peak value. R_u, R_p: number of independent realisations of the input and the scheduling signal respectively. h: number of harmonics in the scheduling signal. $f_h = h\frac{f_s}{N}$: highest excited frequency in the scheduling. $n_{\text{exc}} = n(\mathbb{K}_{\text{exc}})$ is the number of excited frequencies in the excitation signal.

RMS u (mV)	70	70	140	140
P2P p (mV)	350	700	350	700

For 140 mV RMS, a higher level of the nonlinear distortions is observed than for the 70 mV RMS, see Section 5.1. A different P2P level yields a different range of the scheduling signal and, possibly, a different required model structure.

Naming conventions For further reference, the name of a particular data set will be constructed as the concatenation of the following fields $\{u, p, h, N, \text{RMS}, \text{P2P}\}$. For example,

`MS_Harm_h3_N15640_RMS70_P2P700`

is the data set as obtained for a multisine excitation, a harmonic scheduling with 3 excited bins, $N = 15640$ data points in one period, an RMS of 70 mV for the excitation, and a peak-to-peak value of 700 mV for the scheduling. This naming convention is used to name the corresponding data files. The data files, which are of the type `.mat` and saved with Matlab®R2014b, consist of the following six variables:

Name	Description
`u_ref` `p_ref`	the reference input and scheduling signals, fed to the data generators
`u_m` `y_m` `p_m`	the measured input, output, and scheduling signals
`f_s`	the sample frequency

As indicated in Table 1, each data file consists of multiple realisations of the excitation and/or the scheduling signal (denoted R_u and R_p). In the data files, each measured signal u_m, y_m, p_m is given by a matrix with dimensions $(3N) \times (R_u R_p)$. For example, for $R_u = 3$ and $R_p = 2$ we have that, for the first 3 columns, one and the same realisation of $p(t)$ was applied, and for the last 3 columns one other realisation of $p(t)$ was used. For each of the six columns, a different realisation of $u(t)$ was used.

4.4 Benchmark criteria

Each single data file (except those with constant scheduling variables) define an *estimation* and a *validation* data set. If

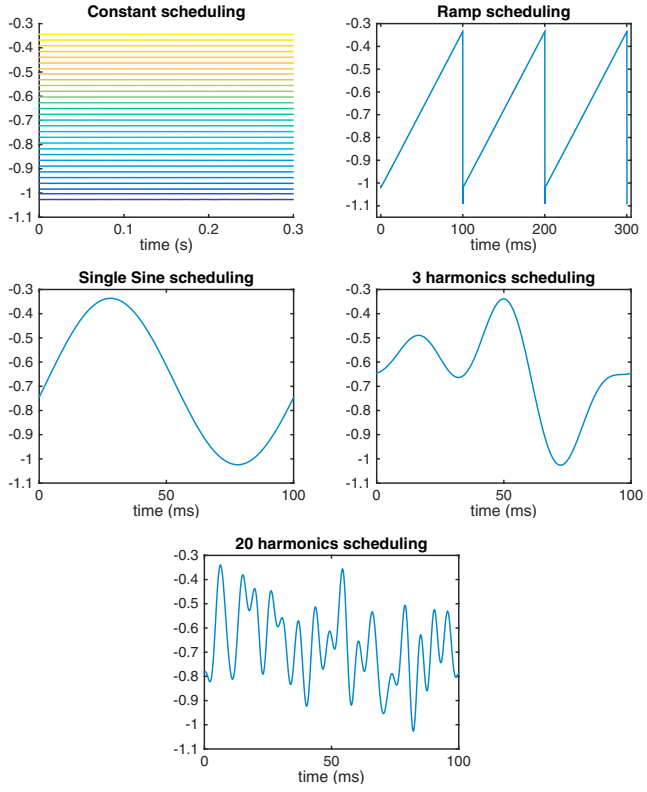

Fig. 4. Scheduling signals, expressed in Volts.

required, the estimation data set can be further split into estimation and calibration data sets.

When considering an LTV model, 3 realisations of the excitation are available with the same scheduling signal, and thus the same time variation. The first two are used for the estimation. The last one is intended for validation.

When considering an LPV model, the purpose is to be able to predict the behaviour of the system for a trajectory of the scheduling signal which was not known during the estimation. A distinction is made between **local** and **global** identification approaches (Tóth, 2010, Chapter 1):

Local approach: One of the data files with constant scheduling variables is used for the estimation, and the validation is performed on one of the realisations in a data file with varying scheduling.

Global approach: A data file with harmonic scheduling is used. The first three realisations have equal trajectories for the scheduling, and are used for the estimation. The validation data set consists of one of the last three realisations in the same data file (which have another trajectory of the scheduling).

Obviously, it is not allowed to use the validation data set during the identification step. The proposed benchmark criterion is given by the RMS error on the *second* period of the simulated output signal (such that the first period can be used to eliminate transient effects):

$$\mathrm{RMSE}_{y_\mathrm{v}} = \sqrt{\frac{1}{N-N_\mathrm{tr}} \sum_{n=N+N_\mathrm{tr}}^{2N-1} \left(y_{m,\mathrm{v}}(n) - y\left(n, \hat{\theta}, u_{m,\mathrm{v}}, p_{m,\mathrm{v}}\right)\right)^2} \tag{3}$$

where n is the discretised time, y is the simulated output signal, computed from $\hat{\theta}$ (the model parameters estimated using the estimation data set), $u_{m,\mathrm{v}}$ and $p_{m,\mathrm{v}}$ (the measured input and scheduling signals from the validation data set). The scheduling signal is to be used for LPV models only. For LTV models that do *not* take into account the periodicity of the time variation, $N_\mathrm{tr} = 500$ is used to eliminate transient effects. Otherwise, $N_\mathrm{tr} = 0$. Further on, benchmark results are included for the data sets with harmonic scheduling variables with 3 and 20 harmonics, on the authors' own LTV and LPV estimators.

5. IDENTIFICATION RESULTS

The results in this section are based on identification algorithms from the authors, and are meant to give a feeling of the dynamic behaviour of the system.

5.1 Constant scheduling

Data set used: `MS_Const_N15640_RMS70_P2P700`.

When applying a constant scheduling, the circuit is behaving time invariantly. The response to a multisine excitation reveals additional information on the system, as shown in Figure 5. The output DFT spectrum is given for different constant values of the scheduling signal, and is indicated by different colours. At the excited frequencies (top dots), the linear contributions follow the shifting resonance frequency. The non-excited harmonics (crosses in the figure), whose bins are given by

$$k_\mathrm{NL} \in \{P_\mathrm{exc}, 2P_\mathrm{exc}, \ldots, N/2\} \setminus \mathbb{K}_\mathrm{exc}, \tag{4}$$

indicate the level of nonlinear distortions, see Schoukens et al. (2009). These lie roughly 45 dB below the linear contributions when the excitation signal has an RMS value of 70 mV (and about 39 dB below for an RMS value of 140 mV, not in the figure). Note that the spectrum of the nonlinear distortions varies with the scheduling parameter. When working in a linear framework, for a time-varying scheduling, this presents an additional challenge: the nonlinear distortions act as a non-stationary disturbance source on the output signal. For a rigorous statistical treatment, this must be taken into account.

The energy at the other spectral lines,

$$k_\mathrm{n} \in \{1, 2, \ldots, N/2\} \setminus \{P_\mathrm{exc}, 2P_\mathrm{exc}, \ldots, N/2\} \tag{5}$$

(small dots at the bottom of the figure) indicate the noise level, which lies about 80 dB below the linear contributions. The maximum likelihood estimator from Pintelon and Schoukens (2012) for continuous-time systems was used to identify the LTI models with orders 1/2, depicted in Figure 2.

5.2 Ramp scheduling, multisine excitation

Data set used: `MS_Ramp_N15640_RMS140_P2P700`.

When applying a multisine excitation with a sparse excited frequency grid to a linear system which is slowly time-varying, a highly structured output spectrum results. This is illustrated in Figure 6, in which case a linearly increasing scheduling is applied to the circuit. As observed, and explained in Lataire et al. (2012), the output spectrum consists of 'skirt' shaped contributions, centred around the excited frequencies.

It has been shown that these skirts contain information on the time variation. The technique proposed in Lataire et al.

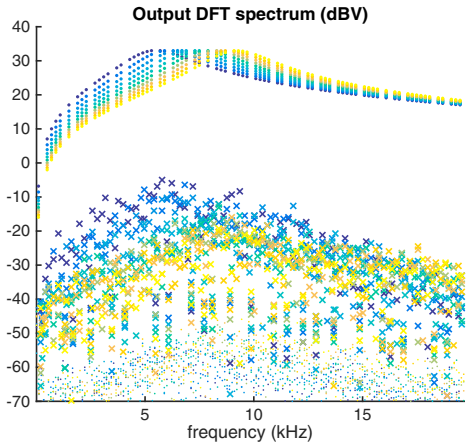

Fig. 5. DFT spectral response to a multisine excitation, for constant scheduling (color code in top left plot of Figure 4). Dots: excited frequencies (linear contribution). Crosses: non-excited harmonics of the multisine (nonlinear contributions). Small dots: non-harmonic bins (noise contributions).

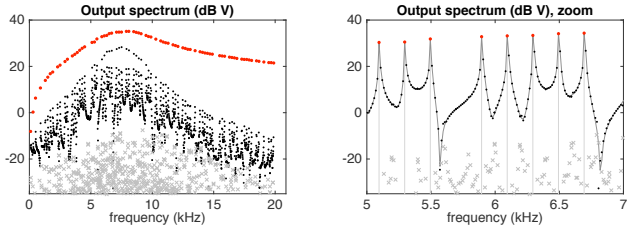

Fig. 6. Output DFT spectrum, for a linearly increasing scheduling variable (ramp). Red dots: excited frequencies. Black dots: non-excited frequencies. Grey crosses: difference between measured and modelled output spectrum.

(2012) is used on this data set to obtain a *semi-parametric* estimate of the instantaneous frequency response function, as given in Figure 7. In this context, semi-parametric means that the model is parametric in the time (the time variation of the transfer function is modelled as a polynomial in time), but non-parametric in the frequency (a polynomial is identified at each individual excited frequency). In Figure 7, the instantaneous FRF is computed at the exited frequencies (red dots), and linearly interpolated at the non-excited ones, as grey shaded lines. The shade of grey of the instantaneous FRF evolves from dark at the beginning of the experiment, to light grey at the end. Keep in mind that, unlike in Section 5.1, this model is obtained via a single experiment, during which the dynamics of the system change with time.

5.3 Scheduling with 3 harmonics

Data set used: `MS_Harm_h3_N15640_RMS70_P2P700`.

The system is identified as a differential equation with time-varying coefficients, *viz.*:

$$\sum_{n=0}^{N_a} a_n(t)\frac{d^n y(t)}{dt^n} = \sum_{n=0}^{N_b} b_n(t)\frac{d^n u(t)}{dt^n}, \tag{6}$$

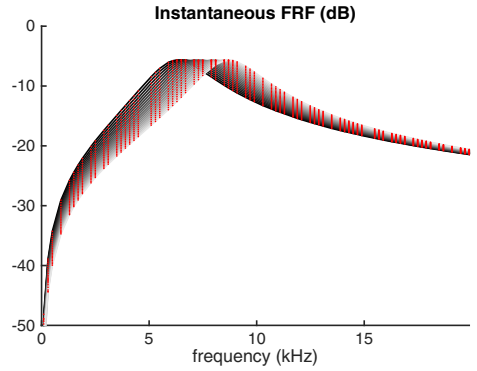

Fig. 7. Identified instantaneous FRF, at excited frequencies (red dots), and linearly interpolated (grey shaded lines).

The estimator is implemented as explained in Lataire and Pintelon (2011). Note that the explicit dependence on the scheduling parameter was not taken into account (that is, the system is identified as being *time*-varying). The model orders were set to $N_a = 3$ and $N_b = 1$. The coefficients $a_n(t)$ and $b_n(t)$ were identified as cubic splines, with derivatives continuous up to 2nd order. In addition, a_0 was constrained to be a constant, and the other coefficients had 15 degrees of freedom.

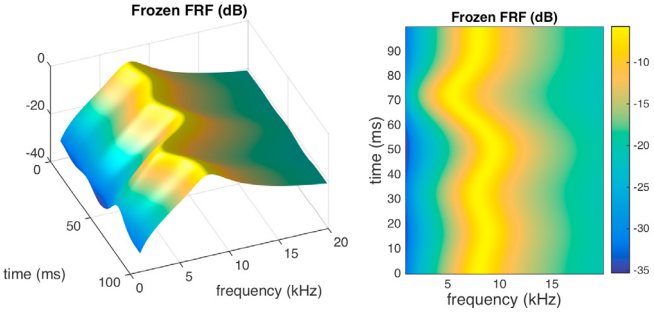

Fig. 8. Evolution of the frozen FRF, with a scheduling signal consisting of the sum of 3 harmonically related sines.

Figure 8 shows the evolution of the estimated frozen FRF, defined at time instant t^* as follows:

$$FRF_{\text{frozen}}(j\omega, t^*) = \frac{\sum_{n=0}^{N_b} b_n(t^*)(j\omega)^n}{\sum_{n=0}^{N_a} a_n(t^*)(j\omega)^n} \tag{7}$$

This is the FRF of the LTI system obtained by freezing the coefficients at time instant t^*. Notice that the evolution of the resonance frequency (peak of the FRF) matches the shape of the scheduling signal (scheduling with 3 harmonics in Figure 4). The benchmark criterion (3) for this estimate on the validation data set is

$$\text{RMSE}_{y_v} = 0.1156\,\text{mV}. \tag{8}$$

(RMS of the measured output signal is 16 mV) Since this estimate does not take into account the periodicity of the time variation, the first 500 samples of the simulated output were discarded.

5.4 Scheduling with 20 harmonics

Data set used: `MS_Harm_h20_N15640_RMS70_P2P700`.

Instead of time-varying, the system is now identified as *parameter* varying, explicitly including the measured scheduling signal as information to the estimator. The model consid-

ered is an ordinary differential equation, whose coefficients depend explicitly on the scheduling signal in a static way:

$$\sum_{n=0}^{N_a} a_n(p(t)) \frac{d^n y(t)}{dt^n} = \sum_{n=0}^{N_b} b_n(p(t)) \frac{d^n u(t)}{dt^n} \tag{9}$$

where the model orders are chosen to be $N_a = 3$ and $N_b = 1$. The coefficients a_n and b_n are identified as 1st order polynomials in $p(t)$. In addition, a_3 was constrained to be constant. More information on this LPV estimator will be made available in future work.

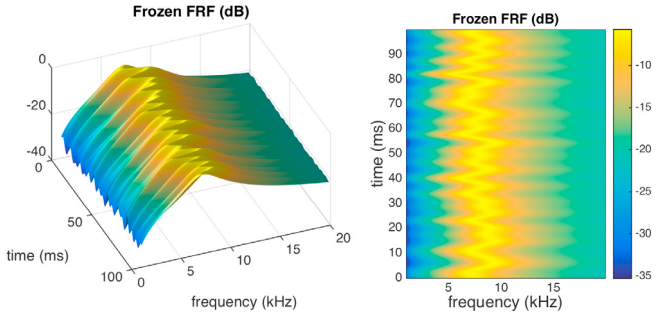

Fig. 9. Evolution of the frozen FRF, with a scheduling signal consisting of the sum of 20 harmonically related sines.

Figure 9 shows the evolution of the estimated frozen FRF, defined at time instant t^* as follows:

$$FRF_{\text{frozen}}(j\omega, t^*) = \frac{\sum_{n=0}^{N_b} b_n(p(t^*))(j\omega)^n}{\sum_{n=0}^{N_a} a_n(p(t^*))(j\omega)^n} \tag{10}$$

This is the FRF of the LTI system obtained by freezing the scheduling parameter at time instant t^*. Again, notice that the evolution of the resonance frequency (peak of the FRF) matches the shape of the scheduling signal (scheduling with 20 harmonics in Figure 4). The benchmark criterion (3) for this estimate on the validation data set is

$$\text{RMSE}_{y_v} = 0.1125\,\text{mV}. \tag{11}$$

(RMS of the measured output signal is 16 mV)

6. CONCLUSION

These benchmark data sets provide experimental data on a fairly simple electronic circuit which embodies a typical example of a linear time- or parameter varying system. A large number of excitation and scheduling configurations are provided. We believe that these data sets can help practitioners in LTV and LPV models with assessing the quality of their estimators.

REFERENCES

Balas, G.J. (2002). Linear, parameter-varying control and its application to a turbofan engine. *International Journal of Robust and Nonlinear Control*, 12(9), 763–796. doi: 10.1002/rnc.704.

Bamieh, B. and Giarre, L. (2002). Identification of linear parameter varying models. *International Journal of Robust and Nonlinear Control*, 12(9), 841–853.

Breugelmans, T., Lataire, J., Muselle, T., Tourwé, E., Pintelon, R., and Hubin, A. (2012). Odd random phase multisine electrochemical impedance spectroscopy to quantify a non-stationary behaviour. theory and validation by calculating an instantaneous impedance value. *Electrochimica Acta*, 76, 375–382.

Caigny, J.D., Camino, J., Oliveira, R., Peres, P., and Swevers, J. (2010). Gain-scheduled H2 and H infinity control of discrete-time polytopic time-varying systems. *IET Control Theory & Applications*, 4(3), 362–380.

Ertveldt, J., Lataire, J., Pintelon, R., and Vanlanduit, S. (2014). Frequency-domain identification of time-varying systems for analysis and prediction of aeroelastic flutter. *Mechanical Systems and Signal Processing*, 47(1-2), 225 – 242. doi:http://dx.doi.org/10.1016/j.ymssp.2013.08.020. MSSP Special Issue on the Identification of Time Varying Structures and Systems.

Fujimori, A. and Ljung, L. (2006). Parameter estimation of polytopic models for a linear parameter varying aircraft system. *Transactions of the Japan Society for Aeronautical and Space Sciences*, 49(165), 129–136.

Hsu, K., Vincent, T., and Poolla, K. (2008). Nonparametric methods for the identification of linear parameter varying systems. In *Computer-Aided Control Systems, 2008. CACSD 2008. IEEE International Conference on*, 846–851.

Lataire, J. and Pintelon, R. (2011). Frequency-domain weighted non-linear least-squares estimation of continuous-time, time-varying systems. *IET Control Theory & Applications*, 5(7), 923–933.

Lataire, J., Pintelon, R., and Louarroudi, E. (2012). Non-parametric estimate of the system function of a time-varying system. *Automatica*, 48(4), 666–672.

Niedzwiecki, M. (2008). Optimal and suboptimal smoothing algorithms for identification of time-varying systems with randomly drifting parameters. *Automatica*, 44(7), 1718 – 1727.

Pintelon, R., Louarroudi, E., and Lataire, J. (2013). Detecting and quantifying the nonlinear and time-variant effects in FRF measurements using periodic excitations. *IEEE Transactions on Instrumentation and Measurement*, 62(12), 3361–3373. doi:10.1109/TIM.2013.2267457.

Pintelon, R. and Schoukens, J. (2012). *System Identification: A Frequency Domain Approach*. John Wiley, 2nd edition.

Schoukens, J., Lataire, J., Pintelon, R., Vandersteen, G., and Dobrowiecki, T. (2009). Robustness issues of the best linear approximation of a nonlinear system. *IEEE Trans. on Instrumentation and Measurement*, 58(5), 1737–1745.

Spiridonakos, M. and Fassois, S. (2009). Parametric identification of a time-varying structure based on vector vibration response measurements. *Mechanical Systems and Signal Processing*, 23(6), 2029 – 2048.

Tóth, R. (2010). *Modeling and Identification of Linear Parameter-Varying Systems*, volume 403 of *Lecture Notes in Control and Information Sciences*. Springer-Verlag, Berlin Heidelberg, first edition.

Tóth, R., Heuberger, P., and Van den Hof, P. (2009). Asymptotically optimal orthonormal basis functions for LPV system identification. *Automatica*, 45(6), 1359–70.

Tóth, R., van de Wal, M., Heuberger, P.S.C., and Van den Hof, P.M.J. (2011). LPV identification of high performance positioning devices. In *Proc. of the American Control Conf.*, 151–158. San Francisco, California, USA.

Verhaegen, M. and Yu, X. (1995). A class of subspace model identification algorithms to identify periodically and arbitrarily time-varying systems. *Automatica*, 31(2), 201 – 216.